Exosomes derived from dental pulp stem cells accelerate cutaneous wound healing by enhancing angiogenesis via the Cdc42/p38 MAPK pathway

ZIYU ZHOU*, JIANMAO ZHENG*, DANLE LIN, RUOMAN XU, YANAN CHEN and XIAOLI HU

Department of Operative Dentistry and Endodontics, Guanghua School of Stomatology, Hospital of Stomatology, Guangdong Provincial Key Laboratory of Stomatology, Sun Yat-sen University, Guangzhou, Guangdong 510055, P.R. China

Received August 22, 2022; Accepted October 18, 2022

DOI: 10.3892/ijmm.2022.5199

Abstract. Skin wound healing is a common challenging clinical issue which requires advanced treatment strategies. The present study investigated the therapeutic effects of exosomes derived from dental pulp stem cells (DPSC-Exos) on cutaneous wound healing and the underlying mechanisms. The effects of DPSC-Exos on cutaneous wound healing in mice were examined by measuring wound closure rates, and using histological and immunohistochemical analysis. A series of functional assays were performed to evaluate the effects of DPSC-Exos on the angiogenic activities of human umbilical vein endothelial cells (HUVECs) *in vitro*. Tandem mass tag-based quantitative proteomics analysis of DPSCs and DPSC-Exos was performed. Gene Ontology and Kyoto Encyclopedia of Genes and Genomes pathway enrichment analyses were used to evaluate the biological functions and pathways for the differentially expressed proteins in DPSC-Exos. Western blot analysis was used to assess the protein levels of cell division control protein 42 (Cdc42) and p38 in DPSC-Exos and in HUVECs subjected to DPSC-Exos-induced angiogenesis. SB203580, a p38 mitogen-activated protein kinase (MAPK) signaling pathway inhibitor, was employed to verify the role of the p38 MAPK pathway *in vitro* and *in vivo*. Histological and immunohistochemical staining revealed that the DPSC-Exos accelerated wound healing by promoting neovascularization. The DPSC-Exos promoted the migration, proliferation and capillary formation capacity of HUVECs. Proteomics data demonstrated that proteins contained in DPSC-Exos regulated vasculature development and angiogenesis. Pathway analysis revealed that proteins expressed in DPSC-Exos were involved in several pathways, including MAPK pathway. Western blot analysis demonstrated that the DPSC-Exos increased the protein levels of Cdc42 and phosphorylation of p38 in HUVECs. SB203580 suppressed the angiogenesis induced by DPSC-Exos. On the whole, the present study demonstrates that DPSC-Exos accelerate cutaneous wound healing by enhancing the angiogenic properties of HUVECs via the Cdc42/p38 MAPK signaling pathway.

Correspondence to: Dr Jianmao Zheng or Professor Xiaoli Hu, Department of Operative Dentistry and Endodontics, Guanghua School of Stomatology, Hospital of Stomatology, Guangdong Provincial Key Laboratory of Stomatology, Sun Yat-sen University, 56 Lingyuan West Road, Guangzhou, Guangdong 510055, P.R. China
E-mail: zhengjm25@mail.sysu.edu.cn
E-mail: huxiaol3@mail.sysu.edu.cn

*Contributed equally

Abbreviations: DPSCs, dental pulp stem cells; HUVECs, human umbilical vein endothelial cells; MSCs, mesenchymal stem cells; Exos, exosomes; TMT, tandem mass tags; GO, Gene Ontology; KEGG, Kyoto Encyclopedia of Genes and Genomes; FBS, fetal bovine serum; PBS, phosphate-buffered saline; H&E, hematoxylin and eosin; Cdc42, cell division control protein 42; MAPK, mitogen-activated protein kinase; FGD5, FYVE, RhoGEF and PH domain containing 5; VEGF, vascular endothelial growth factor; NTA, nanoparticle tracking analysis; TEM, transmission electron microscopy

Key words: exosomes, wound healing, angiogenesis, p38 MAPK pathway, dental pulp stem cells

Introduction

As the largest organ of the human body, the skin provides protection against environmental injury and microbial infection, and has sensory and metabolic functions (1). Injury caused to the skin can cause both physical and mental damage to patients. An impaired skin wound healing process may lead to infection, prolonged wound healing and scarring (2). The classic stages of wound repair include inflammation, new tissue formation and remodeling (3). During the proliferation phase, neoangiogenesis plays a crucial role (4).

Exosomes (Exos) from mesenchymal stem cells (MSCs) originating from bone marrow, adipose tissue and the umbilical cord have been demonstrated to accelerate cutaneous wound healing by enhancing angiogenesis, re-epithelialization and collagen deposition (5-7). Exos are nanovesicles of endocytic origin secreted by the majority of cells in culture, with a diameter of 30-150 nm; they are known as messengers that transmit bioactive molecules, such as nucleic acids and proteins to

the recipient cells for cell-cell communications (8). They contain abundant cargoes which participate in regeneration. From a material science perspective, these nanocarriers with a particular composition of functional molecules are natural carriers, featuring an extraordinarily improved biocompatibility and bioavailability than any conventional manufactured materials (9). Exosomal proteins, such as Jagged 1, Ang-2 and DMBT1 actively participate in therapeutic angiogenesis for tissue repair (10-12). However, the use of stem cells is often limited as the source and harvesting of stem cells is highly invasive. Thus, it may prove useful to search for a new parent cell source from which it may be easier to obtain abundant Exos for tissue repair.

Dental pulp stem cells (DPSCs) exhibit MSC-like behavior, including immense potential for angiogenic effects (13). These cells can be harvested from extracted human third molars non-invasively, and are an extremely accessible cell resource for the development of therapeutic approaches. Although DPSCs are less abundant in tissue, they are easy to culture and expand *in vitro* along with their stemness (14,15). Indeed, accumulating evidence suggests that DPSCs exhibit immense potential in central nervous system repair, stroke recovery, diabetes treatment, muscle regeneration and wound healing (16-18). Exos derived from DPSCs (DPSC-Exos) have been reported to exhibit regenerative therapeutic potential for applications in dental pulp tissue regeneration, neuroprotection and craniofacial bone healing (19-21). Considering that Exos are critical mediators of cell activity, it would be meaningful to explore whether DPSC-Exos have the ability to accelerate the healing process of cutaneous wounds.

The present study thus examined the effects of DPSC-Exos on the angiogenesis of human umbilical vein endothelial cells (HUVECs), which are related to cutaneous wound healing. Tandem mass tag (TMT)-labeled quantitative proteomics analysis was employed to identify the protein expression profiles in DPSC-Exos compared with their parent cells. Gene Ontology (GO) annotation and Kyoto Encyclopedia of Genes and Genomes (KEGG) pathway enrichment analyses were used to evaluate biological functions and pathways for the differentially expressed proteins in DPSC-Exos. The aims of the present study were to clarify the following: i) The role of DPSC-Exos in the cutaneous wound healing *in vivo*; ii) the effects of DPSC-Exos on the angiogenic activities of HUVECs *in vitro*; and iii) the potential signaling pathways involved in the DPSC-Exo-induced angiogenesis of HUVECs.

Materials and methods

Cells and cell culture. The present study was approved by the Ethics Committee of Sun Yat-sen University [No. ERC-(2017)-34]. Human DPSCs were obtained from healthy pulp tissues harvested from wisdom teeth without caries, which were extracted from 10 donors (both male and female, 22-36 years old) between September, 2018 and March, 2019 at the Hospital of Stomatology, Sun Yat-sen University, Guangzhou, China. Dental pulp tissues were minced and digested for the isolation of DPSCs as previously described (22). DPSCs were cultured in α-MEM with 10% fetal bovine serum (FBS; Gibco; Thermo Fisher Scientific, Inc.) and 1% penicillin-streptomycin (MilliporeSigma). HUVECs were purchased from AllCells, LLC and expanded in complete endothelial cell growth medium (EGM; AllCells Biotech Shanghai Co., Ltd.). For the exosome co-culture experiment, 10 μg/ml exosomes were added to the culture medium of HUVECs. All cells were maintained at 37˚C in an incubator contained 5% CO_2.

Exosome isolation and identification. The DPSCs were washed with phosphate-buffered saline (PBS; Biosharp) and incubated in fresh serum-free α-MEM 48 h prior to the isolation of exosomes. The cell culture supernatant was then harvested and subjected to two centrifugation steps (500 x g for 10 min at 25˚C; 2,000 x g for 30 min at 25˚C) to remove dead cells and cell debris. Exosome pellets were purified from the cleared supernatant by ultracentrifugation at 100,000 x g for 1 h at 4˚C. An exosome pellet from about $12x10^6$ cells was resuspended in 100 μl cold PBS. Exosomes were either used immediately or stored at -80˚C until use. The exosome protein concentration was quantified using a BCA Protein Assay kit (Jinan Bocai Chemical Technology Co., Ltd.). The expression levels of the exosomal markers, CD9 and CD63 (Affinity Biosciences) were measured using western blot analysis, as described below. Nanoparticle tracking analysis (NTA) was performed to determine the size distribution of exosomes.

Transmission electron microscopy (TEM). The morphology of the exosomes was visualized using TEM. Exosomes suspended in PBS were placed onto formvar/carbon-coated nickel grids and incubated for 30 min at room temperature. Images of the grids were acquired using an H-7650 transmission electron microscope (Hitachi corporation).

Mouse skin wound model and treatment. All animal experiments were performed in accordance with institutionally approved protocols for animal research (Animal Care and Use Committee of Sun Yat-sen University) (No. SYSU-IACUC-2022-000248). A total of 6 female C57BL/6 mice (8 weeks old; weighing 18-20 g) were purchased from the Guangdong Medical Laboratory Animal Center. Age-matched 8-week-old female mice from the same background were used in the present study. During the experiment, the mice were kept in a specific pathogen-free environment (temperature, 22±2˚C; humidity, 55±10%), with free access to food and water. All mice were anesthetized with an intraperitoneal injection of sodium pentobarbital (75 mg/kg) and euthanized by cervical dislocation, while being deeply anesthetized with sodium pentobarbital. Death verification included the absence of heartbeat, breathing or respiration. In the animal experiments, the humane endpoints was reached when the animal lost 20% of its original weight according to predefined criteria (23,24). In the present study, the maximum percentage of body weight loss observed was not >10%. After shaving, a 1x1 cm full-thickness excision skin wound was created with a pair of surgical scissors, on the backs of the mice. After the surgery on day 1, the 6 mice were randomly divided into two groups and were subcutaneously injected with either DPSC-Exos (120 μg per mouse) as the treatment group or an equal volume of PBS (control group) around the wounds at four equally spaced injection sites.

Wound healing evaluation. To observe the wound healing process, images of the wounds were captured using a digital camera (iPhone 12, Apple) on days 0, 3, 5, 7, 9, 12 and 14, and the wound healing rates were calculated according to the following formula: Wound healing rate (%)=(A0-An)/A0 x100, where 'A0' represents the area of the initial wound (t=day 0) and 'An' represents the residual area of the wound on a the certain day (t=day n). The rates of wound closure were quantified using ImageJ software (v.1.52a, National Institutes of Health).

Hematoxylin and eosin (H&E) and immunohistochemical staining. To examine the formation of new blood vessels, the mice were sacrificed on day 14 post-wounding. The skin specimens were harvested and photographed using a stereomicroscope (MZ10F, Lecia Microsystems GmbH), and then analyzed using H&E and immunohistochemical staining. The use of H&E was preferred for viewing cellular and tissue structure details in the wound area. Hematoxylin precisely stains nuclear components which helps to identify inflammation, while eosin stains cytoplasmic components, including collagen and red blood cells (25-27). Immunostaining for CD31 was utilized to identify the endothelial cells of blood vessels in order to quantify the newly formed blood vessels in the wound. CD31, a 130-kDa glycoprotein expressed on endothelial cells, is commonly used as a biomarker for detecting vascular endothelium (28). The tissues were fixed in 4% paraformaldehyde solution, dehydrated with a series of graded ethanol and embedded in paraffin. The sections (10-μm-thick) were stained with H&E (Wuhan Servicebio Technology Co., Ltd.) or angiogenesis-related protein CD31 (1:600, cat. no. GB11063-2, Wuhan Servicebio Technology Co., Ltd.) to evaluate vascularization. For H&E staining, the sections were stained with hematoxylin for 3 min and eosin for 1 min at room temperature. For the immunohistochemical staining of CD31, the sections were incubated with first antibody at 4˚C overnight, then followed by incubation with the horseradish peroxidase-conjugated anti-rabbit IgG antibody (1:200, cat. no. G1215-3, Wuhan Servicebio Technology Co., Ltd.) for 1 h at room temperature. After rinsing with PBS, the 3,3'-diaminobenzidine (DAB) Staining kit (Wuhan Servicebio Technology Co., Ltd.) was employed with hematoxylin counterstain. The slides were observed and photographed under an epifluorescence microscope (Zeiss AG). To compare the number of newly formed blood vessels from the different groups, five random fields per section near wound edges were counted using Image-Pro Plus 6 software (Media Cybernetics, Inc.).

Exosome uptake assay. To visualize the endocytosis of exosomes by HUVECs, exosomes were stained with PKH26 (MilliporeSigma) according to the manufacturer's instructions. Isolated exosomes were resuspended in 250 μl diluent C, and 1 μl PKH26 was added and immediately mixed by gentle pipetting. The staining was terminated by the addition of an equal volume of exosome-free FBS following incubation for 5 min at room temperature. The mixture was washed twice with PBS by ultracentrifugation (100,000 x g for 1 h at 4˚C) and resuspended in 100 μl exosome-free culture medium. The PKH26-labeled exosomes were then added to the HUVECs and incubated for 24 h at 37˚C. Following incubation with PKH26-labeled exosomes, the cells were washed with PBS for three times and fixed with 4% paraformaldehyde for 10 min at room temperature, the cell nuclei were stained with 4,6-diamidino-2-phenylindole (DAPI) for 5 min at room temperature. The images of fluorescence-labeled exosome internalization were obtained using a confocal laser scanning microscope (Zeiss AG).

Transwell migration assay. For the Transwell migration assay, Transwell inserts with 8-μm pore filters (Corning, Inc.) were used. The HUVECs ($1x10^4$ cells/well) were seeded onto upper chambers containing 200 μl medium supplemented with DPSC-Exos, SB203580 (10 μM; Selleck Chemicals), SB203580 (10 μM) + DPSC-Exos, or PBS. Concurrently, 500 μl cultured medium were added to the bottom chamber and incubated at 37˚C for 24 h. The non-migrated cells in the upper chamber were gently removed using a cotton swab and the lower chamber was fixed with 4% paraformaldehyde for 10 min at room temperature, stained with 0.1% crystal violet (MYM Technologies, Ltd.) for 30 min at room temperature, washed with PBS twice, and imaged using an inversion microscope (Zeiss AG). The quantity of migrated cells was counted and analyzed using ImageJ software (v.1.52a, National Institutes of Health).

Scratch wound assay. The HUVECs ($2x10^5$ cells/well) were plated in 12-well plates and incubated at 37˚C until reaching 90% confluency. The assay was conducted in the absence of serum. A micro-injury was scratched on the monolayer using a 200 μl pipette tip and washed with PBS to remove the debris. The cells were treated with DPSC-Exos, SB203580 (10 μM), SB203580 (10 μM) + DPSC-Exos, or PBS prior to obtaining microscopic images at 0 h. The level of migration was measured by the ratio of closure area to initial wound area (t=0 h) as follows: Migration area (%)=(A0-A6)/A0 x100, where 'A0' represents the area of initial wound area and 'A6' represents the residual area of wound at the metering point after 6 h (t=6 h). The wound area was quantified using ImageJ software (v.1.52a, National Institutes of Health) to calculate the percentage wound closure and the migration rate.

Cell proliferation assay. A Cell Counting Kit-8 (Dojindo Laboratories, Inc.) was used to assess cell proliferation. Concisely, the HUVECs were seeded in 96-well plates ($1x10^3$ cells/well) in EGM supplemented with DPSC-Exos and SB203580 (10 μM). On days 1, 2, 3 and 4, CCK-8 solution was added to HUVECs (10 μl per well) and the cells were incubated at 37˚C for 1 h. The absorbance was measured at 450 nm using a microplate reader (BioTek Instruments, Inc.) and the optical density values represented the proliferation level of the HUVECs.

Tube formation assay. The HUVECs ($1x10^4$ cells/well) were seeded in a 96-well plate coated with 50 μl Matrigel (cat. No. 354277, Corning, Inc.) and treated with DPSC-Exos, SB203580 (10 μM), SB203580 (10 μM) + DPSC-Exos, or PBS, respectively. After 6 h of culture incubation at 37˚C, gels were observed to examine the image of tube formation. The total tube length and total loops were measured as the mean sum

length and loops of capillary-like structures per well using ImageJ software (v.1.52a, National Institutes of Health).

Protein extraction for proteomics analysis. The DPSCs seeded in 75 cm^2 cell culture flasks were incubated in serum-free α-MEM for 48 h at 37˚C and then washed with PBS prior to use. DPSC-Exos were isolated from the culture medium of DPSCs, respectively. Both the DPSCs and DPSC-Exo samples contained three biological replicates. TMT-based quantitative proteomics analysis was conducted by Jingjie PTM BioLab (Hangzhou) Co., Inc. All samples were sonicated on ice in lysis buffer (8 M urea, 1% Protease Inhibitor Cocktail) three times prior to centrifugation (12,000 x g for 10 min) at 4˚C to remove the remaining debris. Subsequently, the supernatant was collected. A BCA protein assay (Beyotime Institute of Biotechnology) was performed to determine the protein concentration.

Trypsin digestion and TMT labeling. The protein solution was reduced with 5 mM dithiothreitol at 56˚C for 30 min, alkylated with 11 mM iodoacetamide (Millipore Sigma) in the dark at room temperature for 15 min, and then diluted with 100 mM tetraethyl ammonium bromide (TEAB; Millipore Sigma) until the urea concentration was <2 M. TEAB is a dissolution buffer for isobaric mass tag labeling experiments (29,30). Trypsin was added to the solution at 1:50 (w/w) trypsin-to-protein mass ratio and incubated at 37˚C overnight, and the trypsin-to-protein mass ratio was then changed to 1:100 (w/w). Following trypsin digestion, the peptide was desalted, vacuum-dried, reconstituted in 0.5 M TEAB, and processed using a TMT kit (Thermo Fisher Scientific, Inc.).

High-performance liquid chromatography (HPLC) fractionation and liquid chromatography-mass spectrometry (LC-MS)/MS analysis. A Thermo Betasil C18 column (5 μm particles, 10 mm ID, 250 mm length; Thermo Fisher Scientific, Inc.) was utilized to fractionate tryptic peptides into fractions using high pH reverse-phase HPLC. In brief, peptides were initially separated with a gradient of 8 to 32% acetonitrile (pH 9.0) over a period of 60 min into 60 fractions, and then combined into six fractions before being dried by vacuum centrifugation (300 x g for 2.5 h at 25˚C).

For LC-MS/MS analysis, the tryptic peptides were dissolved in solvent A (0.1% formic acid) and separated using a homemade reversed-phase analytical column (15-cm length, 75 μm i.d.). The gradient comprised an increase from 6 to 23% solvent B (0.1% formic acid in 98% acetonitrile) over a period of 26 min, 23 to 35% in 8 min and climbing to 80% in 3 min then holding at 80% for the last 3 min. All processes were performed on an EASY-nLC 1000 UPLC system (Thermo Fisher Scientific, Inc.) at a constant flow rate of 400 nl/min. The peptides were subjected to NSI source and analyzed using tandem mass spectrometry (MS/MS) using the UPLC system coupled online to Q ExactiveTM Plus (Thermo Fisher Scientific, Inc.). Intact peptides were detected in the Orbitrap at 70,000 resolution and selected for MS/MS with the NCE setting as 28, the fragments were then detected at a resolution of 17,500. MS and MS/MS spectra were acquired in a data-dependent manner. The automatic gain control (AGC) was set at $5x10^4$. An electrospray voltage of 2.0 kV was applied. The scan range was set from 350 to 1,800 m/z for full scan and the fixed first mass was set as 100 m/z.

Database search and bioinformatics analysis. The acquired MS/MS data were processed using Maxquant search engine (v.1.5.2.8, Max Planck Institute of Biochemistry, Germany). Tandem mass spectra were searched against the human UniProt database concatenated with reverse decoy database. Trypsin/P was designated as the cleavage enzyme; up to four missing cleavages were allowed. The mass tolerance for precursor ions was set to 20 ppm (first search) and 5 ppm (main search), and the mass tolerance for fragment ions to 0.02 Da, respectively. The false discovery rate was adjusted to <1% and a minimum score of 40 was set for the identification of modified peptides.

GO annotation proteome was carried out using the UniProt-GOA database (http://www.ebi.ac.uk/GOA/). Proteins were classified by GO annotation into three categories: Biological Process, Cellular Compartment and Molecular Function. InterProScan was used for the functional annotation of identified protein domains based on protein sequence alignment and the InterPro (http://www.ebi.ac.uk/interpro/) domain database. For functional enrichment analysis, the KEGG, http://www.genome.jp/kaas-bin/kaas_main) and GO (http://geneontology.org/) were applied.

Determination and inhibition of the p38 mitogen-activated protein kinase (MAPK) signaling pathway. A pharmacological p38 MAPK inhibitor (SB203580; Selleck Chemicals), was used to assess the participation of the MAPK signaling pathway in the DPSC-Exo-induced effects on HUVECs. The compound was resuspended to 10 mM in dimethyl sulfoxide (DMSO; MP Biomedicals France) and used at 10 μM. For control treatments (0 μM) 0.1% DMSO was used. For experiments assessing the expression of target proteins using western blot analysis, the HUVECs were plated in six-well plates and pre-treated with 10 μM SB203580 for 6 h. Since SB203580 inhibited p38 MAPK catalytic activity instead of the phosphorylation of p38, the effects of SB203580 on the p38 MAPK pathway were assessed by the expression of hsp27 as a substrate (31).

To determine the participation of the MAPK signaling pathway in the therapeutic effect of DPSC-Exos on cutaneous wound healing *in vivo*, a total of 12 age-matched 8-week-old female C57BL/6 mice were randomly divided into four groups as follows: PBS + vehicle, PBS + SB203580, DPSC-Exos + vehicle and DPSC-Exos + SB203580 group. After the cutaneous wound had been formed for 6 h, mice in the PBS/DPSC-Exos + SB203580 group were administered an intraperitoneal injection of SB203580 (5 mg/kg). The SB203580 was dissolved in the vehicle (4% DMSO + 30% PEG300 + 5% Tween-80 + 61% ddH_2O) according to the manufacturer's instructions. The dose of SB203580 was selected from a previous study (32).

Western blot analysis. Total protein was extracted from either DPSCs or HUVECs using RIPA buffer (Jinan Bocai Chemical Technology Co., Ltd.) and quantified using a BCA Protein Assay kit (Jinan Bocai Chemical Technology Co., Ltd.). The protein samples (5 μg per lane) were electrophoresed with 4-20% Bis-Tris sodium dodecyl sulfate polyacrylamide gel and transferred onto a 0.2 μm PVDF membrane (MilliporeSigma). After blocking with 5% (w/v) non-fat milk for 1 h at room

temperature, the membranes were incubated with diluted primary antibodies overnight at 4˚C. The primary antibodies and concentrations used in the present study were as follows: Phosphorylated (p-)p38 (1:1,000; cat. no. 4511, Cell Signaling Technology, Inc.), p38 (1:1,000; cat. no. 8690, Cell Signaling Technology, Inc.), p-hsp27 (1:1,000; cat. no. AF3080), hsp27 (1:1,000; cat. no. AF6082), cell division control protein 42 (Cdc42; 1:1,000; cat. no. DF6322), β-tubulin (1:8,000; cat. no. AF7011), FYVE, RhoGEF and PH domain containing 5 (FGD5; 1:500; cat. no. DF13013), CD63 (1:1,000; cat. no. AF5117), CD9 (1:1,000; cat. no. AF5139) (all from Affinity Biosciences) and β-actin (1:8,000; cat. no. MA5-11869, Invitrogen; Thermo Fisher Scientific, Inc.). Subsequently, the membranes were washed with Tris-buffered saline with Tween-20 (TBST) and incubated with goat anti-rabbit IgG-HRP (1:2,000; cat. no. As006, Asbio Technology, Inc.) as the secondary antibody for 1 h at room temperature. Bands on the blots were visualized using GeneGnome XRQ (Syngene). ImageJ software (v.1.52a, National Institutes of Health) was utilized to quantify the density of the bands.

Statistical analysis. All experiments were performed with at least three replicates per group and each *in vitro* experiment was repeated three times. All values are expressed as the mean ± standard deviation (SD). Differences between two groups were evaluated using an unpaired Student's t-test and those between more than two groups were compared using one-way ANOVA with a Bonferroni post hoc test using SPSS 25.0 software (IBM Corp.). $P<0.05$ was considered to indicate a statistically significant difference.

Results

Identification of DPSC-Exos. DPSC-Exos were characterized using TEM, western blot analysis and NTA. TEM images revealed that the vesicles isolated from the culture supernatant of the DPSCs exhibited a spherical morphology (Fig. S1A). Western blot analysis demonstrated that these vesicles were positive for the exosomal surface markers, CD9 and CD63 (Fig. S1B). The results of NTA revealed that the diameters of these nanoparticles ranged from 50-100 nm (Fig. S1C). Taken together, these results confirmed their identity as exosomes.

DPSC-Exos promote cutaneous wound healing in mice by promoting angiogenesis. The present study investigated the effects of DPSC-Exos on cutaneous wound healing using a full-thickness wound model on mice. A significantly more rapid wound closure rate was observed when DPSC-Exos were injected (Fig. 1A and B). Skin images from the underside of the wounds, which were collected 14 days post-wounding demonstrated that the mice treated with the DPSC-Exos exhibited a greater amount of newly formed blood vessels compared to the control group (Fig. 1C). Furthermore, H&E and immunohistochemical staining was performed at the wound site. A considerable amount of capillary-structure blood vessels (Fig. 1D and E) and a higher expression of CD31 in the DPSC-Exo-treated group (Fig. 1F and G) confirmed that the DPSC-Exos enhanced local angiogenesis. These findings suggested that the DPSC-Exos accelerated wound healing *in vivo* by promoting angiogenesis.

DPSC-Exos enhance the angiogenic activities of HUVECs. To examine the effects of DPSC-Exos on HUVECs behavior *in vitro*, the internalization of exosomes into these cells was first monitored. Following 24 h of incubation with PKH26-labeled DPSC-Exos, fluorescence microscopy analysis revealed red fluorescent spots in the cytoplasm around the nucleus of HUVECs, which indicated that the HUVECs were able to take up DPSC-Exos (Fig. 2A). For functional analysis, the present study then assessed how DPSC-Exos modulated HUVEC angiogenesis, including migration, proliferation and tube formation. Transwell migration assay (Fig. 2B and C) and scratch wound assay revealed that the DPSC-Exos significantly increased the motility of HUVECs (Fig. 2D and E). CCK-8 assay was utilized to examine the proliferation of the cells within 4 days of culture time, which revealed that the DPSC-Exos increased the proliferative capacity of the HUVECs (Fig. 2F). DPSC-Exo treatment also improved tube formation in the HUVECs as the total tube length and total loops increased in the DPSC-Exo-treated group (Fig. 2G-I). On the whole, these results indicated that the DPSC-Exos enhanced the migration, proliferation and tube formation ability of HUVECs.

Proteomics analysis of DPSCs and DPSC-Exos. Since the mechanisms involved in the promoting effects of DPSC-Exos on angiogenesis remained unknown, the present study employed TMT-labeled quantitative proteomics analysis to identify the protein expression profiles in DPSC-Exos compared with their parent cells. All proteins and peptides identified and quantified using LC-MS/MS in DPSC-Exos and DPSCs are presented in Table SI. A total of 4,592 proteins were quantified, including 1,159 upregulated and 460 downregulated proteins (Fig. 3A). In addition, a volcano plot illustrating the statistically sizable difference of expressed proteins between DPSC-Exos and DPSCs was constructed (Fig. 3B). A change in differential expression levels exceeding 1.5 was regarded as the change threshold for significance.

To thoroughly determine the proteins obtained in these data, GO analysis and KEGG pathway analysis were performed to classify the biological functions and their characteristics, as well as their molecular interaction networks. The results of GO classification analysis revealed that proteins involved in various biological processes in relation to wound healing, such as positive regulation of cell motility, migration, proliferation, vasculature development and angiogenesis, were markedly increased in the DPSC-Exos (Fig. 3C). KEGG pathway analysis revealed that proteins contained in DPSC-Exos were involved in several pathways, including the MAPK signaling pathway (Fig. 3D and Table SII). As shown in Fig. 3E, tubulin was used as an internal control to normalize the western blot analysis data. The ratios of Cdc42, p38 and p-p38 protein levels to tubulin expression were used for comparisons. HUVECs were treated with DPSC-Exos and a significant increase was found in the expression of Cdc42 and p-p38 (Fig. 3E and F). Cdc42 is required for the activation of p38 and plays a key role in cell migration and proliferation (33,34). Taken together, these findings prompted the hypothesis that the Cdc42/p38 MAPK signaling pathway may play an essential role in DPSC-Exo-induced angiogenesis.

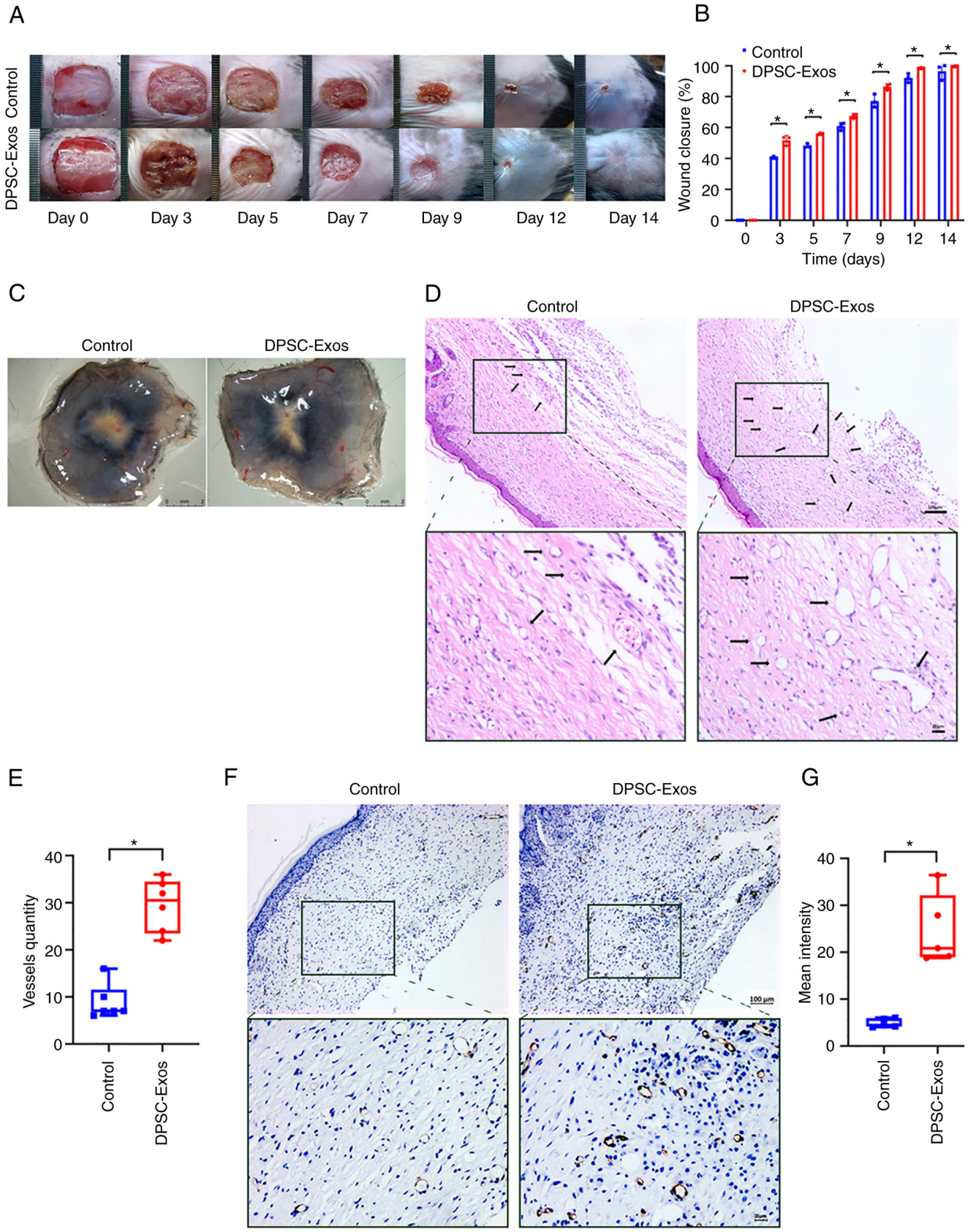

Figure 1. DPSC-Exos accelerate cutaneous wound healing in mice by promoting angiogenesis. (A) Gross view and quantification of wound area of mice treated with PBS and DPSC-Exos on days 3, 5, 7, 9, 12 and 14 post-wounding. Scale bar, 1 cm. (B) The rate of wound closure in wounds receiving DPSC-Exos treatments was significantly higher at the indicated time points (n=3). (C) Gross view of wounds of mice treated with PBS and DPSC-Exos on day 14 post-wounding from the undersurface. More newly formed blood vessels were detected in the wound sites of the DPSC-Exo-treated group. Scale bar, 2 mm. (D and E) Hematoxylin & eosin staining of the wound sections treated with PBS and DPSC-Exos on day 14 after the operation. The black arrows indicate newly formed blood vessels. The vessel quantity in the DPSC-Exo-treated group was larger than that of the control group (n=3). Scale bar, 100 μm. (F and G) Immunohistochemical staining for CD31 in wound sections of mice treated with PBS and DPSC-Exos at 14 days after the operation. A higher expression of CD31 was found in the DPSC-Exo-treated group (n=3). Scale bar, 100 μm. *P<0.05. DPSC, dental pulp stem cell; Exo, exosome; PBS, phosphate-buffered saline.

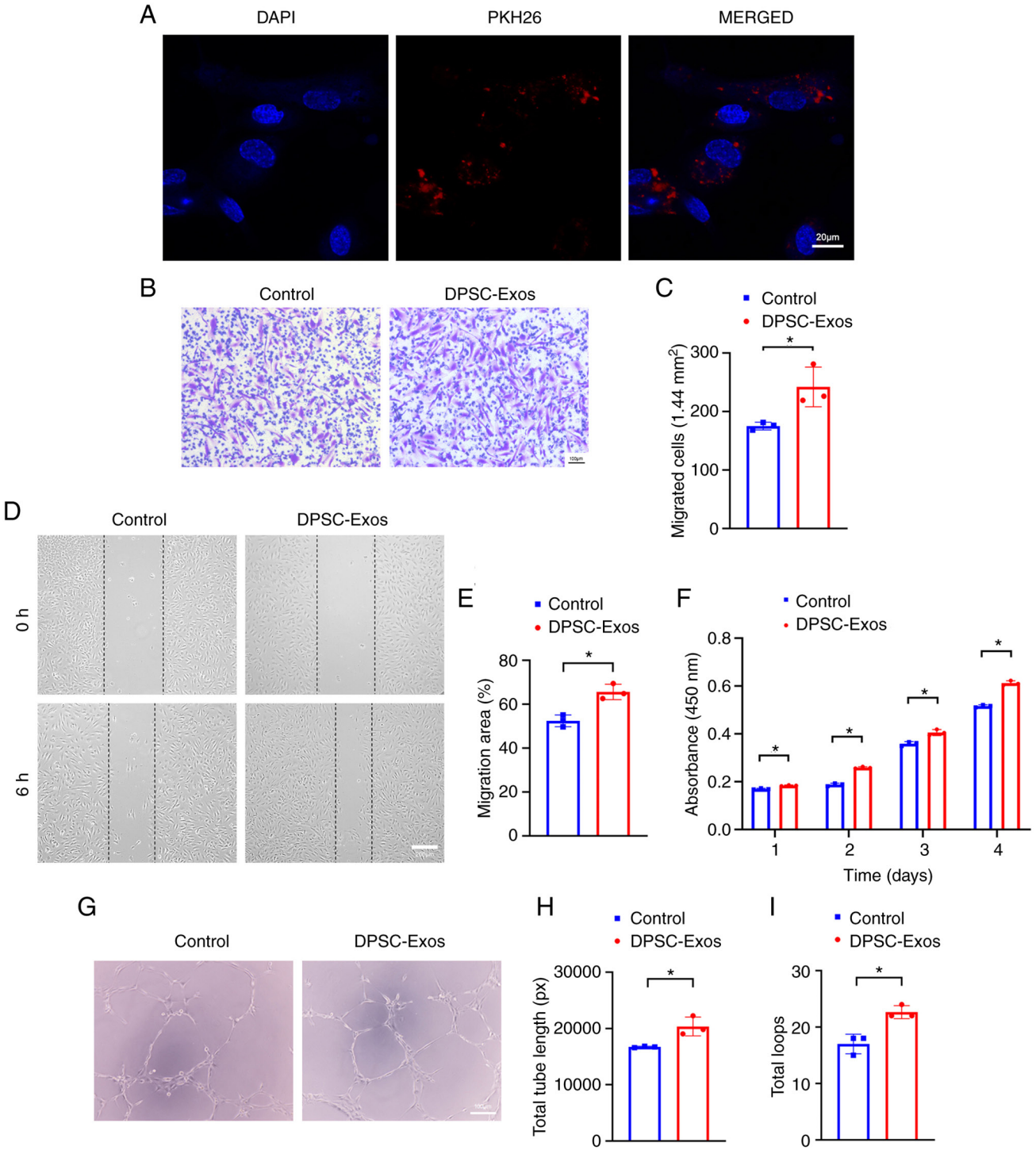

Figure 2. DPSC-Exos enhance the angiogenic activities of HUVECs. (A) Endocytosis of exosomes by HUVECs was visualized using fluorescent staining with PKH26. (B and C) The migration of HUVECs stimulated by DPSC-Exos was increased (n=3). Scale bar, 100 μm. (D and E) Representative images of scratch wound assay in HUVECs treated with DPSC-Exos or PBS. The remaining area of the DPSC-Exo-treated group was smaller than that of the control group (n=3). Scale bar, 100 μm. (F) The proliferation of HUVECs receiving different treatments was examined using CCK-8 assay. The DPSC-Exo-treated group exhibited a greater proliferative capacity than the control group (n=3). (G-I) Representative images of the tube formation assay on Matrigel in HUVECs treated with DPSC-Exos or PBS. The total tube length and quantity of total loops in DPSC-Exo-treated group were larger than those of the control group (n=3). Scale bar, 100 μm. *P<0.05. DPSC, dental pulp stem cell; Exo, exosome; HUVEC, human umbilical vein endothelial cell; PBS, phosphate-buffered saline.

Of note, the proteomics data indicated that the expression of FGD5, a pro-angiogenesis protein, was 2.299-fold higher in the DPSC-Exos than in the DPSCs (Table SIII). FGD5 is known to mediate pro-angiogenic action of vascular endothelial growth factor (VEGF) in human vascular endothelial cells by inducing the activation of Cdc42 (35). In the present study, as shown in Fig. 3G, β-actin was used as an internal control to normalize the western blot analysis data. The ratios of the FGD5 protein level to β-actin expression were used for comparisons. Western blot analysis also verified that FGD5 was enriched in the DPSC-Exos (Fig. 3G), which may be a potential candidate mediating pro-angiogenic function of DPSC-Exos.

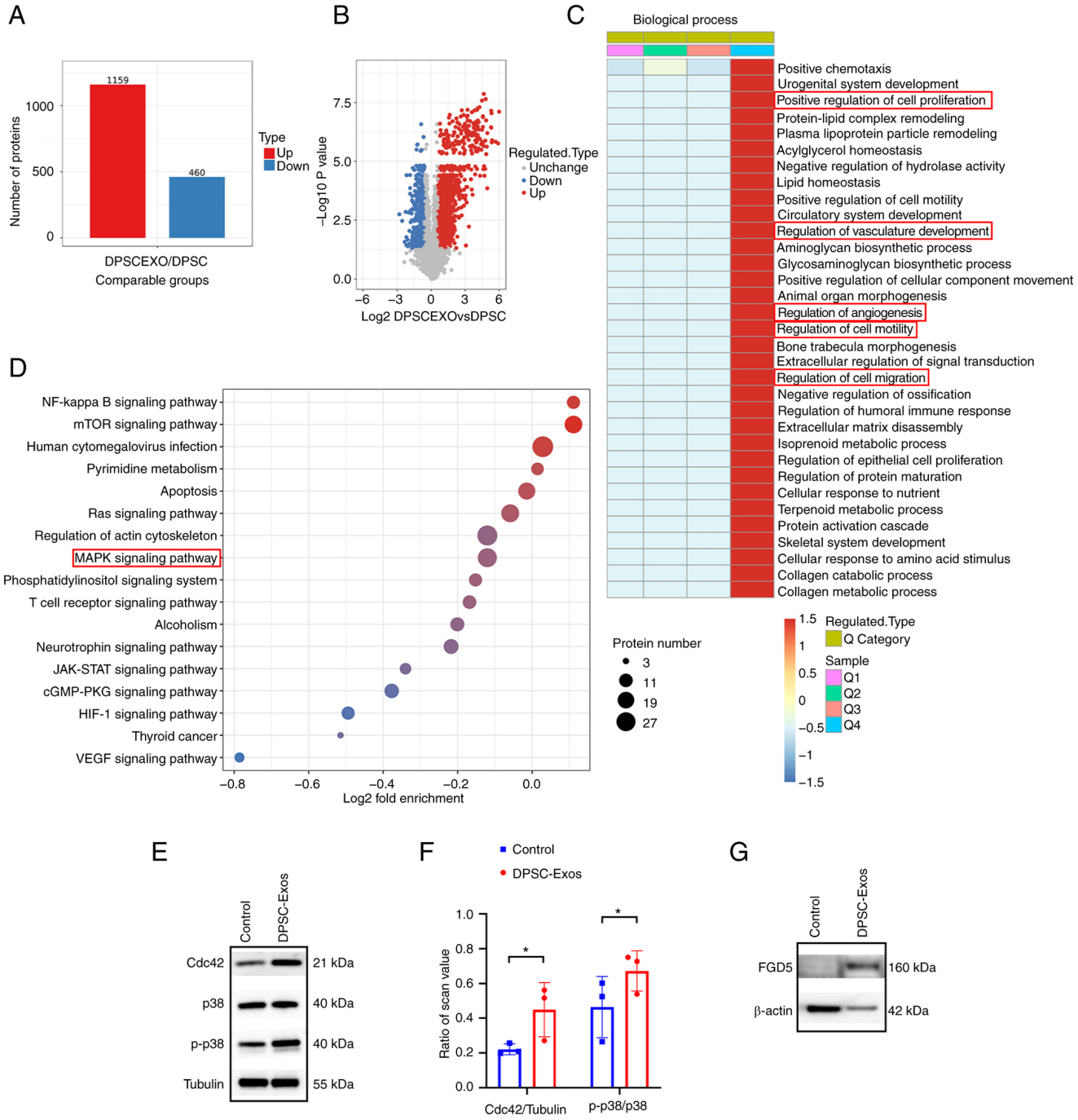

Figure 3. Expression and function of the proteins identified by TMT-labeled quantitative proteomic in DPSC-Exos. (A) The number of differentially expressed proteins in DPSC-Exos compared with DPSCs was identified using TMT-labeled quantitative proteomics analysis. (B) Volcano map of differentially expressed proteins. (C) Differentially expressed proteins were categorized according to the biological process (Gene Ontology term) they were involved in; several of these were related to wound healing. (D) Kyoto Encyclopedia of Genes and Genomes pathway analysis of DPSC-Exos revealed that the enriched proteins involved in multiple signal transductions, including the MAPK signaling pathway. (E and F) The expression of Cdc42, p38 and p-p38 in HUVECs was higher following treatment with DPSC-Exos (n=3). *P<0.05. (G) Western blot analysis of pro-angiogenic protein (FGD5) and cytosolic marker (β-actin) expression from DPSC and DPSC-Exos. TMT, tandem mass tags; DPSC, dental pulp stem cell; Exo, exosome; p-, phosphorylated; MAPK, mitogen-activated protein kinase; HUVEC, human umbilical vein endothelial cell; Cdc42, cell division control protein 42; FGD5, FYVE, RhoGEF and PH domain containing 5.

Inhibition of the p38 MAPK signaling pathway decreases DPSC-Exo-induced angiogenesis. To examine whether the p38 MAPK signaling pathway is involved in DPSC-Exo-induced angiogenesis, HUVECs were treated with SB203580 to inhibit the p38 MAPK pathway prior to stimulation with the DPSC-Exos. hsp27 is a terminal substrate of the p38 MAPK pathway (36,37), which is related to the positive regulation of angiogenesis, as well as the positive regulation of blood vessel endothelial cell migration (38). In the present study, as shown in Fig. 4A, tubulin was used as an internal control to normalize the western blot analysis data. The ratios of p38, p-p38, hsp27, p-hsp27 protein levels to tubulin expression were used for comparisons. Once the p38 MAPK signaling pathway was inhibited by SB203580, the protein levels of hsp27 and p-hsp27 were significantly decreased in the HUVECs (Fig. 4A). The ratio of p-p38/p-38 and p-hsp27/hsp27 was also

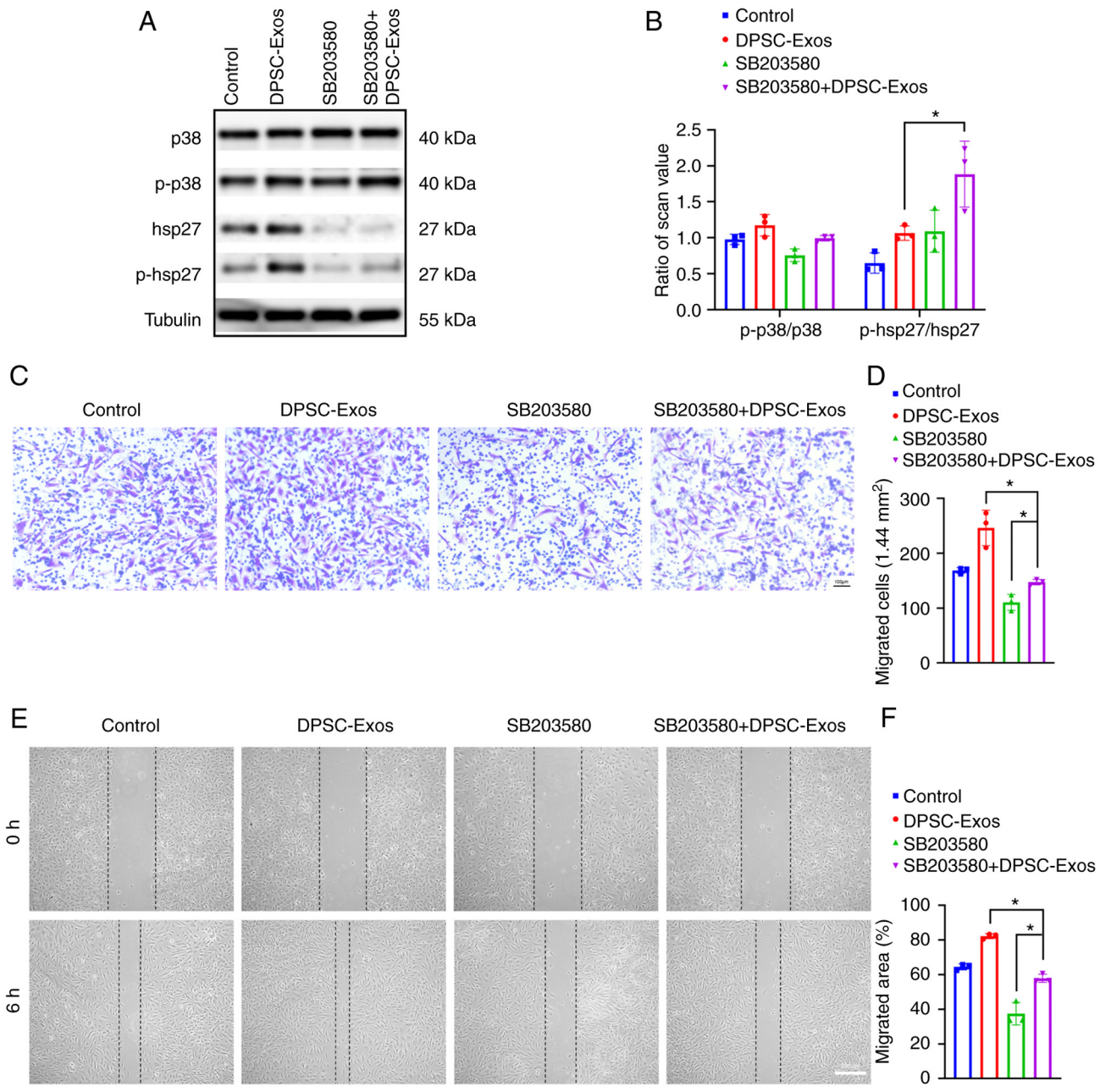

Figure 4. Continued.

shown (Fig. 4B). Transwell migration assay (Fig. 4C and D) and scratch wound assay (Fig. 4E and F) revealed a decreased capacity of the DPSC-Exos to promote cell migration when the HUVECs were pre-treated with SB203580. As shown by CCK-8 assay, the proliferation of the HUVECs which was promoted by DPSC-Exos was also suppressed by the inhibition of p38 by SB203580 (Fig. 4G). In addition, as shown by the results of tube formation assay, the enhanced tube formation ability of the HUVECs stimulated with the DPSC-Exos was reduced by SB203580 (Fig. 4H-J). These outcomes all confirmed that the p38 MAPK signaling pathway was involved in DPSC-Exo-induced angiogenesis.

Inhibition of the p38 MAPK signaling pathway attenuates the therapeutic and pro-angiogenic effects of DPSC-Exos. The present study also examined the effects of p38 inhibition on the healing process of murine cutaneous wounds. The subcutaneous injection of DPSC-Exos accelerated the cutaneous wound closure rate, while this therapeutic effect was attenuated after the p38 MAPK signaling pathway was blocked by SB203580 (Fig. 5A and B). the wound closure rate in all groups reached almost 100% on day 14; thus, a statistically significant difference was not observed at this time point. On the other hand, wounds in the DPSC-Exos + vehicle group were almost completely closed on day 12, which exhibited a much more rapid healing rate than other three groups. Skin images from the underside of the wounds were collected 14 days post-wounding. Compared with the DPSC-Exos + vehicle group, treatment with SB203580 attenuated the development of newly formed blood vessels, as shown in the DPSC-Exos + SB203580 group (Fig. 5C). The quantification of newly formed blood vessels was performed

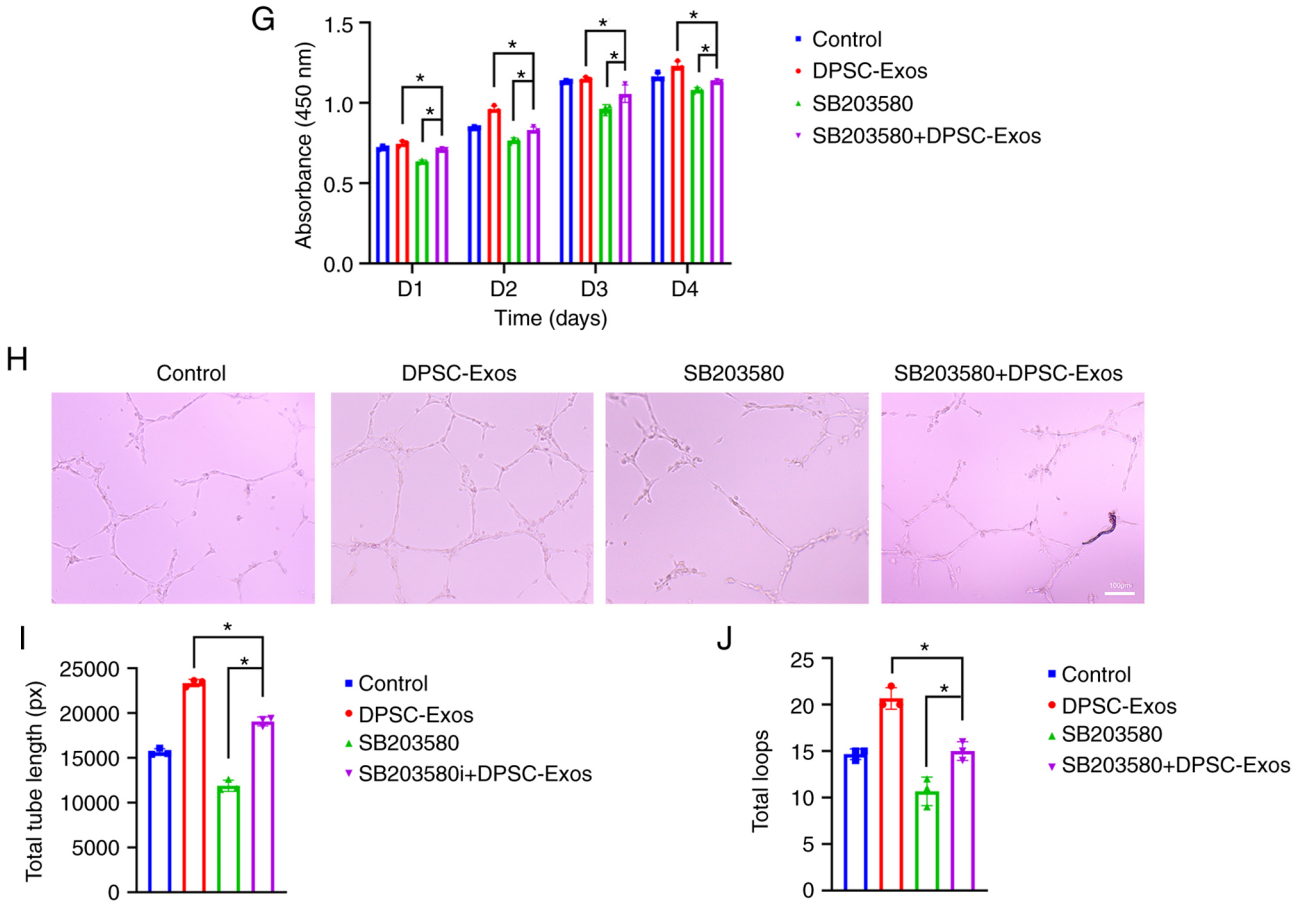

Figure 4. DPSC-Exos promote angiogenesis via p38 MAPK to promote wound healing. (A and B) HUVECs were treated with DPSC-Exos in the presence or absence of SB203580. The expression of p38, p-p38, hsp27 and p-hsp27 was detected using western blot analysis (n=3). (C and D) The migration of HUVECs stimulated by DPSC-Exos or an equal volume of PBS in the presence or absence of SB203580 (n=3). Scale bar, 100 μm. (E and F) Representative images of scratch wound assay in HUVECs treated with DPSC-Exos or PBS in the presence or absence of SB203580 (n=3). Scale bar, 100 μm. (G) The proliferation of HUVECs receiving different treatments were examined using CCK-8 assay (n=3). (H-J) Representative images of the tube formation assay on Matrigel in HUVECs treated with DPSC-Exos or PBS (n=3). Scale bar, 100 μm. *P<0.05. DPSC, dental pulp stem cell; Exo, exosome; p-, phosphorylated; MAPK, mitogen-activated protein kinase; HUVEC, human umbilical vein endothelial cell; hsp27, heat shock protein 27; PBS, phosphate-buffered saline.

using H&E and immunohistochemical staining. With the presence of SB203580, the amount of capillary-structure blood vessels (Fig. 5D and E) and the expression of CD31 (Fig. 5F and G) were suppressed in the mice treated with either PBS or DPSC-Exos. The formed vessels and positive rate of CD31 were decreased in the DPSC-Exos + SB203580 group as compared to the DPSC-Exos + vehicle group. Accordingly, these results substantiated that DPSC-Exo-induced angiogenesis was attenuated by the inhibition of the p38 MAPK signaling pathway *in vivo*.

Discussion

The present study, to the best of our knowledge, is the first to demonstrate that DPSC-Exos could effectively enhanced the functional properties of HUVECs and accelerated cutaneous wound healing in mice. In the process of angiogenesis induced by DPSC-Exos, the Cdc42/p38 MAPK pathway played a crucial role, as the pro-angiogenic effects of DPSC-Exos were attenuated by the inhibition of the p38 MAPK pathway (Fig. 6).

In the present study, it was found that DPSC-Exos accelerated cutaneous wound healing by enhancing the development of new blood vessels in the wound site. As all mice used were female, and estrogen levels can affect the rate of wound healing, more care should be taken in the selection of female animals for future studies, as the levels of estrogens and progesterone cab affect rate of wound healing (39). The results of the present study are unlikely to be affected, since the animal groups were created by chance and the likelihood of the effects of the estrous cycle on outcomes would have averaged out. As has been reported, DPSC-Exos exhibit great potential in bone regeneration, neuroprotection and anti-inflammation (40-42). In a previous study by the authors, DPSC-Exos were found to promote odontogenic differentiation via the TGFβ1/smad signaling pathway by downregulating latent TGF-β-binding protein 1 (LTBP1) (22). The present study demonstrated that the injection of DPSC-Exos triggered angiogenesis by evaluating the vascular marker, CD31, in the wound site. Angiogenesis at the wound site is a critical determinant of wound healing processes, since neovascularization ensures oxygen and nutrition delivery, thus establishing a favorable environment for wound healing. The stimulation of new blood vessel development is a helpful therapeutic target for tissue regeneration.

Recently, exosomes from hypoxia-preconditioned human adipose MSCs have been found to carry >30 types of

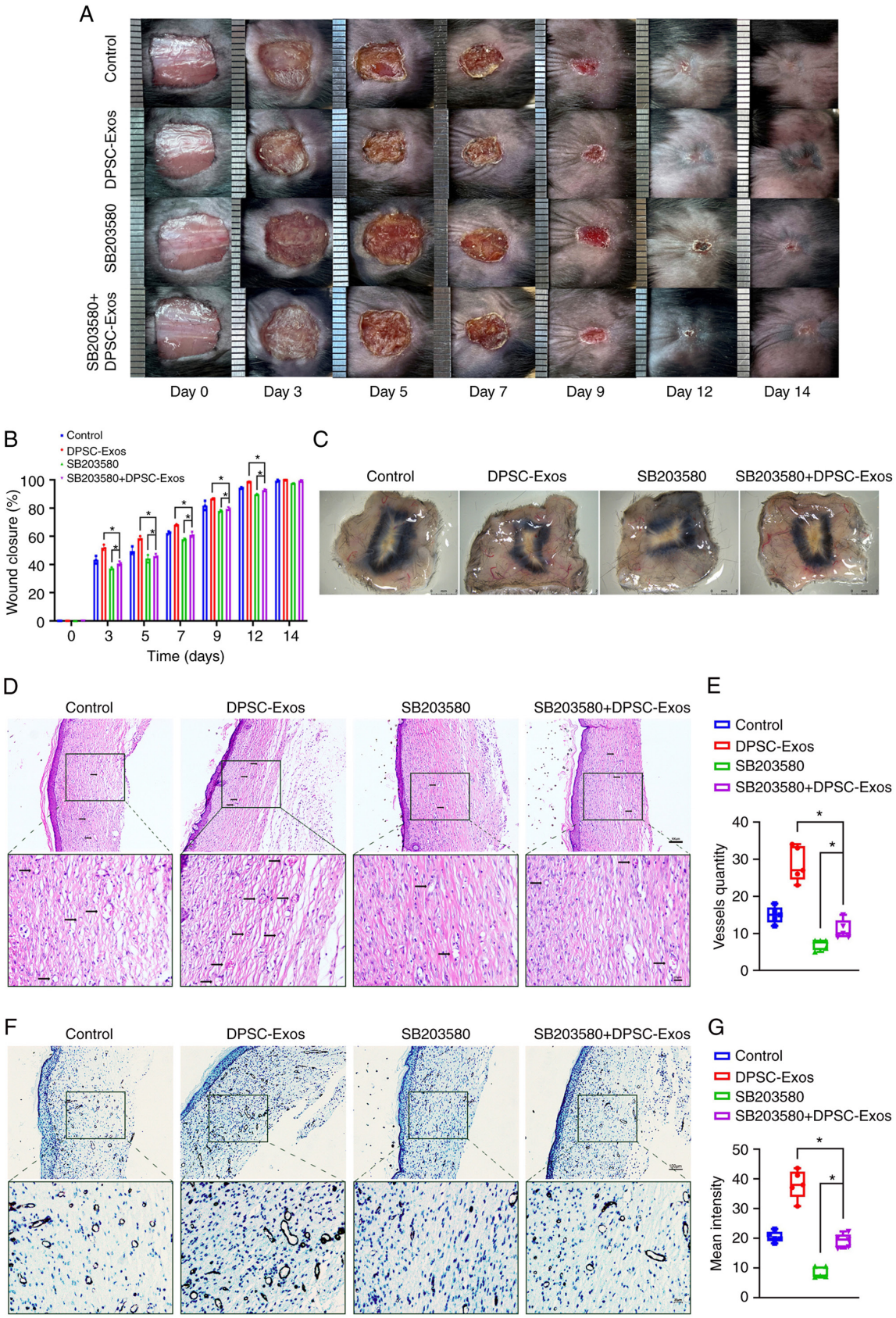

Figure 5. DPSC-Exos accelerate cutaneous wound healing in mice via p38 MAPK. (A) Gross view and quantification of the wound area of mice treated with DPSC-Exos in the presence or absence of SB203580 on days 3, 5, 7, 9, 12 and 14 post-wounding. Scale bar, 1 cm. (B) The rate of wound closure in wounds receiving DPSC-Exos or PBS treatments in the presence or absence of SB203580 at the indicated time points (n=3). (C) Gross view of wounds treated with PBS and DPSC-Exos in the presence or absence of SB203580 on day 14 post-wounding from the undersurface. Scale bar, 2 mm. (D and E) Hematoxylin and eosin staining of wound sections treated with PBS and DPSC-Exos in the presence or absence of SB203580 at 14 days after the operation (n=3). The black arrows indicate newly formed blood vessels. Scale bar, 100 μm. (F and G) Immunohistochemical staining for CD31 in wound sections treated with PBS and DPSC-Exos in the presence or absence of SB203580 at 14 days after the operation (n=3). Scale bar, 100 μm. *P<0.05. DPSC, dental pulp stem cell; Exo, exosome; MAPK, mitogen-activated protein kinase; PBS, phosphate-buffered saline.

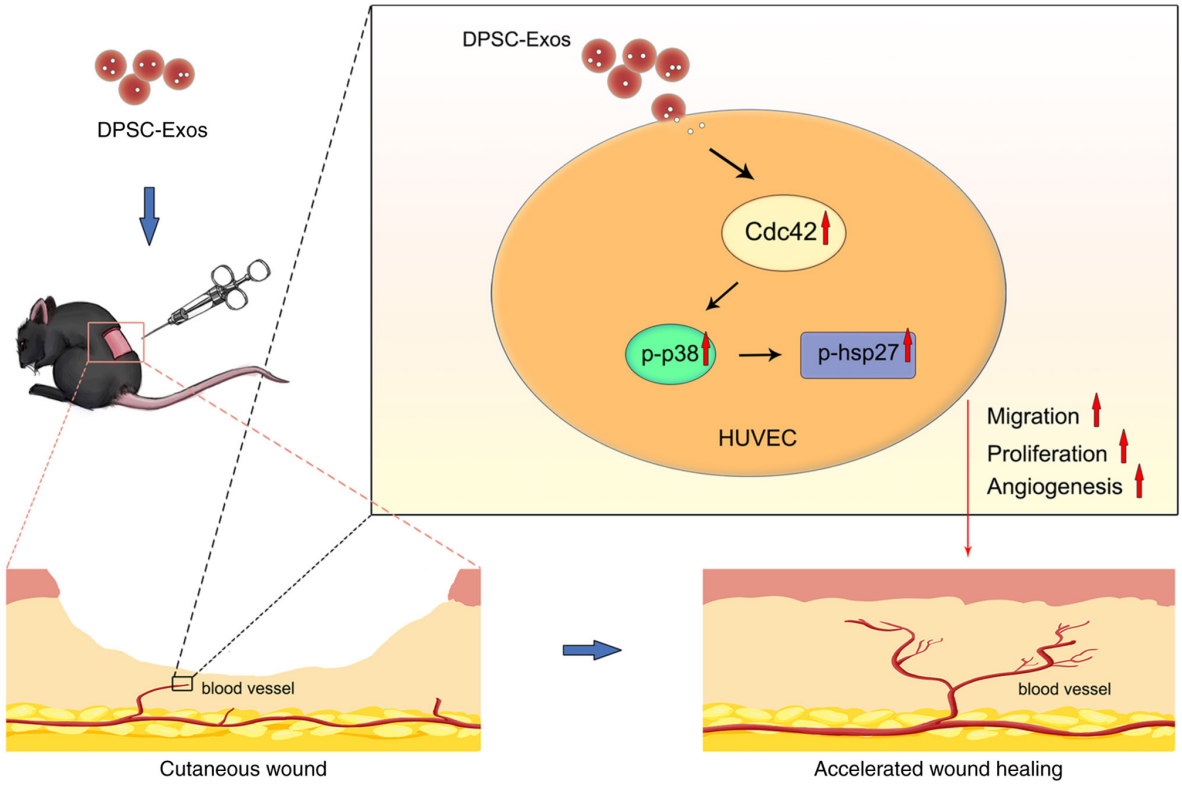

Figure 6. Schematic diagram of the function of DPSC-Exos in accelerating cutaneous wound healing in mice by promoting the angiogenesis of HUVECs via the Cdc42/p38 MAPK signaling pathway. DPSC, dental pulp stem cell; Exo, exosome; HUVECs, human umbilical vein endothelial cells; MAPK, mitogen-activated protein kinase; Cdc42, cell division control protein 42; p-, phosphorylated.

angiogenesis-related proteins and improve neovascularization around the graft tissue (43). Exosomes from MSCs derived from the human umbilical cord, expressing α2M, TLN1, ANK1 and other proteins, are involved in damage repairing (44). In the present study, proteomics analysis revealed that 1,619 differentially expressed proteins were detected in DPSC-Exos. This suggested that there may be potential functional proteins among these, which are involved in different processes of wound healing, and are thus worthy of further exploration.

GO term enrichment analysis revealed that the DPSC-Exos were enriched in the proteins that are involved in the regulation of wound healing-related biological processes, such as the positive regulation of cell motility, migration, proliferation, vasculature development and angiogenesis. Additionally, several *in vitro* experiments were conducted to demonstrate that DPSC-Exos effectively enhanced the migration, proliferation and tube formation ability of HUVECs. New blood vessel formation, which involves endothelial cell proliferation, migration and branching to form capillaries, requires a dynamic regulated interaction between endothelial cells, angiogenesis factors and the surrounding extracellular matrix (45). It is known that some exosomes can regulate the angiogenic function of recipient endothelial cells by transferring exosomal proteins, RNAs and miRNAs into the cytoplasm of these cells (46). Such exosomes represent a highly attractive delivery vehicle for any proteins or RNAs through which they can exert their therapeutic effects.

Previous studies have demonstrated that MSC-Exos can facilitate wound repair; however, some of the underlying mechanisms remain unclear (44,47,48). The present study focused on identifying the underlying mechanisms through which the infusion of DPSC-Exos initiates endothelial cell-mediated wound healing. KEGG pathway analysis revealed that exosomal proteins were enriched in several pathways, including the MAPK pathway. Western blot analysis confirmed that the DPSC-Exos induced significant increases in the protein levels of Cdc42 and the phosphorylation of p38 in HUVECs. Cdc42 is a Rho-family GTPase regulating actin dynamics and cell proliferation (49). Moreover, it is an important activator of the p38 MAPK pathway (50). The sequential activation of the Cdc42/p38 MAPK signaling pathway is essential for VEGF-induced actin reorganization in HUVECs (51,52). Previous studies have indicated that p38 MAPK activation mediates the angiogenesis of endothelial cells by modulating cell migration and proliferation (36,53). Thus, it was hypothesized that DPSC-Exos increased the angiogenic activities of HUVECs through the p38 MAPK pathway. It was found that the stimulation of DPSC-Exos increased the angiogenic activities of HUVECs, whereas these effects were attenuated with the inhibition of the p38 MAPK signaling pathway. Consistent with the phenomenon observed *in vitro*, the *in vivo* experiment with the SB203580 inhibitor illustrated that blocking the p38 MAPK signaling pathway diminished DPSC-Exo-induced angiogenesis in the wound site. SB203580 was used at 10 μM in *in vitro* experiments, and for the *in vivo* experiments, SB203580 at 5 mg/kg dissolved in the vehicle was used according to the manufacturer's instructions, which has been proven to be non-toxic (32,54,55). Taken together, the findings demonstrated that DPSC-Exos increased the migration, proliferation and capillary formation capacity of

endothelial cells via the Cdc42/p38 MAPK signaling pathway, thereby enhancing cutaneous wound healing in mice.

It has been reported that exosomal proteins can activate the p38 MAPK pathway and promote angiogenesis (56). Moreover, the AKT/mTOR, JAK2/STAT3 and PKA signaling pathways are associated with MSC-exo-induced angiogenesis (57-59). The data of the present study confirmed that the positive effects of DPSC-Exos on angiogenesis were not entirely abolished by the inhibition of the p38 MAPK signaling pathway both *in vitro* and *in vivo*, which suggested that other pathways are involved in the regulation of neovascularization.

Furthermore, the present study sought to determine the key component that participates in the modulation of DPSC-Exo-stimulated angiogenic activities of HUVECs. It was found that the expression of FGD5, a pro-angiogenic protein, was markedly higher in DPSC-Exos. FGD5, known to be conducive to pro-angiogenesis processes in endothelial cells, is a Rho guanine-nucleotide exchange factor (Rho GEF) which catalyzes the exchange of GDP for GTP and leads to the activation of its target Rho protein Cdc42 (60). A previous study demonstrated that FGD5 regulates Cdc42 activity and plays a key role in the mediation of the proangiogenic action of VEGF (35). The FGD5-mediated activation of Cdc42 in endothelial cells can protect VEGFR2 from degradation and regulates cytoskeletal dynamics (61). Thus, based on such mechanisms provided by previous research, it was hypothesized that exosomal FGD5 from DPSC-Exos may accelerate cutaneous wound healing by enhancing angiogenesis through the Cdc42/p38 MAPK signaling pathway. To investigate the molecular mechanisms of FGD5 from DPSC-Exos on the angiogenesis of HUVECs, future studies are required.

In conclusion, the present demonstrated that DPSC-Exos promoted the angiogenic properties of endothelial cells via theCdc42/p38 MAPK signaling pathway, thereby enhancing cutaneous wound healing in mice. DPSC-Exo based therapy may possibly represent a useful tool in the field of soft tissue regeneration. However, further studies are required before DPSC-Exo can be used in clinical practice.

Acknowledgements

Not applicable.

Funding

The present study was supported by the National Natural Science Foundation of China (grant nos. 11772361 and 81700950), and the Guangdong Basic and Applied Basic Research Foundation (grant nos. 2022A1515011266 and 2022A1515012531).

Availability of data and materials

The datasets used and/or analyzed during the current study are available from the corresponding author on reasonable request.

Authors' contributions

XH and JZ designed the study. ZZ and JZ performed the experiments and collected the data. DL, RX and YC assisted with the experiments. ZZ analyzed the data and prepared the manuscript. XH and JZ revised the manuscript. All authors have read and approved the manuscript. XH and JZ confirm the authenticity of all the raw data.

Ethic approval and consent to participate

The present study was approved by the Ethics Committee of Sun Yat-sen University [No. ERC-(2017)-34]. Animal experiments followed the Ethical Guidelines for Laboratory Animal Welfare determined by the Institutional Animal Care and Use Committee, Sun Yat-Sen University (no. SYSU-IACUC-2022-000248).

Patient consent for publication

Not applicable.

Competing interests

The authors declare that they have no competing interests.

References

1. Strecker-McGraw MK, Jones TR and Baer DG: Soft tissue wounds and principles of healing. Emerg Med Clin North Am 25: 1-22, 2007.
2. Rodrigues M, Kosaric N, Bonham CA and Gurtner GC: Wound healing: A cellular perspective. Physiol Rev 99: 665-706, 2019.
3. Gurtner GC, Werner S, Barrandon Y and Longaker MT: Wound repair and regeneration. Nature 453: 314-321, 2008.
4. Li J, Zhang YP and Kirsner RS: Angiogenesis in wound repair: Angiogenic growth factors and the extracellular matrix. Microsc Res Tech 60: 107-114, 2003.
5. Ding J, Wang X, Chen B, Zhang J and Xu J: Exosomes derived from human bone marrow mesenchymal stem cells stimulated by deferoxamine accelerate cutaneous wound healing by promoting angiogenesis. Biomed Res Int 2019: 9742765, 2019.
6. Li X, Xie X, Lian W, Shi R, Han S, Zhang H, Lu L and Li M: Exosomes from adipose-derived stem cells overexpressing Nrf2 accelerate cutaneous wound healing by promoting vascularization in a diabetic foot ulcer rat model. Exp Mol Med 50: 1-14, 2018.
7. Hu Y, Rao SS, Wang ZX, Cao J, Tan YJ, Luo J, Li HM, Zhang WS, Chen CY and Xie H: Exosomes from human umbilical cord blood accelerate cutaneous wound healing through miR-21-3p-mediated promotion of angiogenesis and fibroblast function. Theranostics 8: 169-184, 2018.
8. Théry C, Zitvogel L and Amigorena S: Exosomes: Composition, biogenesis and function. Nat Rev Immunol 2: 569-579, 2002.
9. Yang B, Chen Y and Shi J: Exosome biochemistry and advanced nanotechnology for next-generation theranostic platforms. Adv Mater 31: e1802896, 2019.
10. Gonzalez-King H, García NA, Ontoria-Oviedo I, Ciria M, Montero JA and Sepúlveda P: Hypoxia inducible factor-1α potentiates jagged 1-mediated angiogenesis by mesenchymal stem cell-derived exosomes. Stem Cells 35: 1747-1759, 2017.
11. Liu J, Yan Z, Yang F, Huang Y, Yu Y, Zhou L, Sun Z, Cui D and Yan Y: Exosomes derived from human umbilical cord mesenchymal stem cells accelerate cutaneous wound healing by enhancing angiogenesis through delivering angiopoietin-2. Stem Cell Rev Rep 17: 305-317, 2021.
12. Chen CY, Rao SS, Ren L, Hu XK, Tan YJ, Hu Y, Luo J, Liu YW, Yin H, Huang J, *et al*: Exosomal DMBT1 from human urine-derived stem cells facilitates diabetic wound repair by promoting angiogenesis. Theranostics 8: 1607-1623, 2018.
13. Tsutsui TW: Dental pulp stem cells: Advances to applications. Stem Cells Cloning 13: 33-42, 2020.
14. Yoon JK, Kang ML, Park JH, Lee KM, Shin YM, Lee JW, Kim HO and Sung HJ: Direct control of stem cell behavior using biomaterials and genetic factors. Stem Cells Int 2018: 8642989, 2018.

15. Kim BC, Bae H, Kwon IK, Lee EJ, Park JH, Khademhosseini A and Hwang YS: Osteoblastic/cementoblastic and neural differentiation of dental stem cells and their applications to tissue engineering and regenerative medicine. Tissue Eng Part B Rev 18: 235-244, 2012.
16. Botelho J, Cavacas MA, Machado V and Mendes JJ: Dental stem cells: Recent progresses in tissue engineering and regenerative medicine. Ann Med 49: 644-651, 2017.
17. Martínez-Sarrà E, Montori S, Gil-Recio C, Núñez-Toldrà R, Costamagna D, Rotini A, Atari M, Luttun A and Sampaolesi M: Human dental pulp pluripotent-like stem cells promote wound healing and muscle regeneration. Stem Cell Res Ther 8: 175, 2017
18. Mead B, Logan A, Berry M, Leadbeater W and Scheven BA: Concise review: Dental pulp stem cells: A novel cell therapy for retinal and central nervous system repair. Stem Cells 35: 61-67, 2017
19. Huang CC, Narayanan R, Alapati S and Ravindran S: Exosomes as biomimetic tools for stem cell differentiation: Applications in dental pulp tissue regeneration. Biomaterials 111: 103-115, 2016
20. Jarmalavičiūtė A, Tunaitis V, Pivoraitė U, Venalis A and Pivoriūnas A: Exosomes from dental pulp stem cells rescue human dopaminergic neurons from 6-hydroxy-dopamine-induced apoptosis. Cytotherapy 17: 932-939, 2015.
21. Swanson WB, Zhang Z, Xiu K, Gong T, Eberle M, Wang Z and Ma PX: Scaffolds with controlled release of pro-mineralization exosomes to promote craniofacial bone healing without cell transplantation. Acta Biomater 118: 215-232, 2020.
22. Hu X, Zhong Y, Kong Y, Chen Y, Feng J and Zheng J: Lineage-specific exosomes promote the odontogenic differentiation of human dental pulp stem cells (DPSCs) through TGFβ1/smads signaling pathway via transfer of microRNAs. Stem Cell Res Ther 10: 170, 2019.
23. Izar B, Tirosh I, Stover EH, Wakiro I, Cuoco MS, Alter I, Rodman C, Leeson R, Su MJ, Shah P, *et al*: A single-cell landscape of high-grade serous ovarian cancer. Nat Med 26: 1271-1279, 2020.
24. Rochereau N, Roblin X, Michaud E, Gayet R, Chanut B, Jospin F, Corthésy B and Paul S: NOD2 deficiency increases retrograde transport of secretory IgA complexes in Crohn's disease. Nat Commun 12: 261, 2021.
25. Fornabaio G, Barnhill RL, Lugassy C, Bentolila LA, Cassoux N, Roman-Roman S, Alsafadi S and Bene FD: Angiotropism and extravascular migratory metastasis in cutaneous and uveal melanoma progression in a zebrafish model. Sci Rep 8: 10448, 2018.
26. Goerge T, Ho-Tin-Noe B, Carbo C, Benarafa C, Remold-O'Donnell E, Zhao BQ, Cifuni SM and Wagner DD: Inflammation induces hemorrhage in thrombocytopenia. Blood 111: 4958-4964, 2008.
27. Marcinkiewicz AL, Lieknina I, Kotelovica S, Yang X, Kraiczy P, Pal U, Lin YP and Tars K: Eliminating factor H-Binding activity of borrelia burgdorferi CspZ combined with virus-like particle conjugation enhances its efficacy as a lyme disease vaccine. Front Immunol 9: 181, 2018.
28. Albelda SM, Muller WA, Buck CA and Newman PJ: Molecular and cellular properties of PECAM-1 (endoCAM/CD31): A novel vascular cell-cell adhesion molecule. J Cell Biol 114: 1059-1068, 2018.
29. Ju Lee H, Bartsch D, Xiao C, Guerrero S, Ahuja G, Schindler C, Moresco JJ, Yates JR III, Gebauer F, Bazzi H, *et al*: A post-transcriptional program coordinated by CSDE1 prevents intrinsic neural differentiation of human embryonic stem cells. Nat Commun 8: 1456, 2017.
30. Zeng H, Castillo-Cabrera J, Manser M, Lu B, Yang Z, Strande V, Begue D, Zamponi R, Qiu S, Sigoillot F, *et al*: Genome-wide CRISPR screening reveals genetic modifiers of mutant EGFR dependence in human NSCLC. Elife 19: e50223,2019.
31. Kumar S, Jiang MS, Adams JL and Lee JC: Pyridinylimidazole compound SB 203580 inhibits the activity but not the activation of p38 mitogen-activated protein kinase. Biochem Biophys Res Commun 263: 825-831, 2017.
32. Tu GW, Ju MJ, Zheng YJ, Hao GW, Ma GG, Hou JY, Zhang XP, Luo Z and Lu LM: CXCL16/CXCR6 is involved in LPS-induced acute lung injury via P38 signalling. J Cell Mol Med 23: 5380-5389, 2019.
33. Liu Z, Wu H, Jiang K, Wang Y, Zhang W, Chu Q, Li J, Huang H, Cai T, Ji H, *et al*: MAPK-Mediated YAP activation controls mechanical-tension-induced pulmonary alveolar regeneration. Cell Rep 16: 1810-1819, 2016.
34. Koch S and Claesson-Welsh L: Signal transduction by vascular endothelial growth factor receptors. Cold Spring Harb Perspect Med 2: a006502, 2012.
35. Kurogane Y, Miyata M, Kubo Y, Nagamatsu Y, Kundu RK, Uemura A, Ishida T, Quertermous T, Hirata KI and Rikitake Y: FGD5 mediates proangiogenic action of vascular endothelial growth factor in human vascular endothelial cells. Arterioscler Thromb Vasc Biol 32: 988-996, 2012.
36. Rousseau S, Houle F, Landry J and Huot J: p38 MAP kinase activation by vascular endothelial growth factor mediates actin reorganization and cell migration in human endothelial cells. Oncogene 15: 2169-2177, 1997.
37. Armstrong SC, Delacey M and Ganote CE: Phosphorylation state of hsp27 and p38 MAPK during preconditioning and protein phosphatase inhibitor protection of rabbit cardiomyocytes. J Mol Cell Cardiol 31: 555-567, 1999.
38. Evans IM, Britton G and Zachary IC: Vascular endothelial growth factor induces heat shock protein (HSP) 27 serine 82 phosphorylation and endothelial tubulogenesis via protein kinase D and independent of p38 kinase. Cell Signal 20: 1375-1384, 2008.
39. Zhou T, Yang Z, Chen Y, Chen Y, Huang Z, You B, Peng Y and Chen J: Estrogen accelerates cutaneous wound healing by promoting proliferation of epidermal keratinocytes via Erk/Akt signaling pathway. Cell Physiol Biochem 38: 959-968, 2016.
40. Xie L, Guan Z, Zhang M, Lyu S, Thuaksuban N, Kamolmattayakul S and Nuntanaranont T: Exosomal circLPAR1 promoted osteogenic differentiation of homotypic dental pulp stem cells by competitively binding to hsa-miR-31. Biomed Res Int 2020: 6319395, 2020.
41. Venugopal CKS, Rai KS, Pinnelli VB, Kutty BM and Dhanushkodi A: Neuroprotection by human dental pulp mesenchymal stem cells: From billions to nano. Curr Gene Ther 18: 307-323, 2018.
42. Pivoraitė U, Jarmalavičiūtė A, Tunaitis V, Ramanauskaitė G, Vaitkuvienė A, Kašėta V, Biziulevičienė G, Venalis A and Pivoriūnas A: Exosomes from human dental pulp stem cells suppress carrageenan-induced acute inflammation in mice. Inflammation 38: 1933-1941, 2015.
43. Han Y, Ren J, Bai Y, Pei X and Han Y: Exosomes from hypoxia-treated human adipose-derived mesenchymal stem cells enhance angiogenesis through VEGF/VEGF-R. Int J Biochem Cell Biol 109: 59-68, 2019.
44. Bakhtyar N, Jeschke MG, Herer E, Sheikholeslam M and Amini-Nik S: Exosomes from acellular Wharton's jelly of the human umbilical cord promotes skin wound healing. Stem Cell Res Ther 9: 193, 2018.
45. Tonnesen MG, Feng X and Clark RA: Angiogenesis in wound healing. J Investig Dermatol Symp Proc 5: 40-46, 2000.
46. Ribeiro MF, Zhu H, Millard RW and Fan GC: Exosomes function in pro- and anti-angiogenesis. Curr Angiogenes 2: 54-59, 2013.
47. Wu P, Zhang B, Shi H, Qian H and Xu W: MSC-exosome: A novel cell-free therapy for cutaneous regeneration. Cytotherapy 20: 291-301, 2018.
48. Yu M, Liu W, Li J, Lu J, Lu H, Jia W and Liu F: Exosomes derived from atorvastatin-pretreated MSC accelerate diabetic wound repair by enhancing angiogenesis via AKT/eNOS pathway. Stem Cell Res Ther 11: 350, 2020.
49. Liu S, Uppal H, Demaria M, Desprez PY, Campisi J and Kapahi P: Simvastatin suppresses breast cancer cell proliferation induced by senescent cells. Sci Rep 5: 17895, 2015.
50. Liu J, He X, Corbett SA, Lowry SF, Graham AM, Fässler R and Li S: Integrins are required for the differentiation of visceral endoderm. J Cell Sci 122: 233-242, 2009.
51. Lamalice L, Houle F, Jourdan G and Huot J: Phosphorylation of tyrosine 1214 on VEGFR2 is required for VEGF-induced activation of Cdc42 upstream of SAPK2/p38. Oncogene 23: 434-445, 2004.
52. Lamalice L, Houle F and Huot J: Phosphorylation of Tyr1214 within VEGFR-2 triggers the recruitment of Nck and activation of Fyn leading to SAPK2/p38 activation and endothelial cell migration in response to VEGF. J Biol Chem 281: 34009-34020, 2006.
53. Feng PC, Ke XF, Kuang HL, Pan LL, Ye Q and Wu JB: BMP2 secretion from hepatocellular carcinoma cell HepG2 enhances angiogenesis and tumor growth in endothelial cells via activation of the MAPK/p38 signaling pathway. Stem Cell Res Ther 10: 237, 2019.
54. Correa AR, Berbel AC, Papa MP, Morais AT, Peçanha LM and Arruda LB: Dengue virus directly stimulates polyclonal B cell activation. PLoS One 10: e0143391, 2015.
55. Morrison VL, James MJ, Grzes K, Cook P, Glass DG, Savinko T, Lek HS, Gawden-Bone C, Watts C, Millington OR, *et al*: Loss of beta2-integrin-mediated cytoskeletal linkage reprogrammes dendritic cells to a mature migratory phenotype. Nat Commun 5: 5359, 2014.

56. Maji S, Chaudhary P, Akopova I, Nguyen PM, Hare RJ, Gryczynski I and Vishwanatha JK: Exosomal annexin II promotes angiogenesis and breast cancer metastasis. Mol Cancer Res 15: 93-105, 2017.
57. Liang B, Liang JM, Ding JN, Xu J, Xu JG and Chai YM: Dimethyloxaloylglycine-stimulated human bone marrow mesenchymal stem cell-derived exosomes enhance bone regeneration through angiogenesis by targeting the AKT/mTOR pathway. Stem Cell Res Ther 10: 335, 2019.
58. Zhou X, Yan T, Huang C, Xu Z, Wang L, Jiang E, Wang H, Chen Y, Liu K, Shao Z and Shang Z: Melanoma cell-secreted exosomal miR-155-5p induce proangiogenic switch of cancer-associated fibroblasts via SOCS1/JAK2/STAT3 signaling pathway. J Exp Clin Cancer Res 37: 242, 2018.
59. Xue C, Shen Y, Li X, Li B, Zhao S, Gu J, Chen Y, Ma B, Wei J, Han Q and Zhao RC: Exosomes derived from hypoxia-treated human adipose mesenchymal stem cells enhance angiogenesis through the PKA signaling pathway. Stem Cells Dev 27: 456-465, 2018.
60. Park S, Guo Y, Negre J, Preto J, Smithers CC, Azad AK, Overduin M, Murray AG and Eitzen G: Fgd5 is a rac1-specific Rho GEF that is selectively inhibited by aurintricarboxylic acid. Small GTPases 12: 147-160, 2021.
61. Heldin J, O'Callagha n P, Vera RH, Fuchs PF, Gerwins P and Kreuger J: FGD5 sustains vascular endothelial growth factor A (VEGFA) signaling through inhibition of proteasome-mediated VEGF receptor 2 degradation. Cell Signal 40: 125-132, 2017.